Determination of Darcian permeability of porous material by infrared spectrometry

Nicolas Gascoin, Guillaume Fau, Philippe Gillard

J Porous Mater
DOI 10.1007/s10934-011-9478-5

Determination of Darcian permeability of porous material by infrared spectrometry

Nicolas Gascoin · Guillaume Fau · Philippe Gillard

Abstract The active cooling of aerospace structures can be performed by the use of porous materials. It requires characterizing its permeability to predict the cooling efficiency by means of Computational Fluid Dynamics codes. The Darcian term is generally deduced experimentally from a relationship between the mass flow rate and the pressure drop through the porous media. Due to thermo-chemical process involved in the cooling, the permeability can change. It is currently not possible with common techniques to determine these variations during the flight. This paper presents a novel approach taking advantage of well known flow behaviour in chemical reactor engineering in order to propose a real-time in situ quantification of the Darcian permeability. The residence time distribution is analyzed thanks to tracer injection and to associated experimental measures of Infra-Red signals. The IR peak characteristics (height, width, surface, rising and falling gradients) and time delays are analyzed and correlated to physical parameters (mass flow rate, injected mass of tracer, properties of fluids). The peak height and surface and the rising gradient vary linearly in the same sense as the injected tracer mass while the falling gradient varies in the opposite sense. Both gradients decrease with a mass flow rate increase. The time delay between injection and detection of the tracer is quite constant except when changing the fluid nature. A design of experiments allowed estimating quantitatively the influence of each physical parameter on the optical one of the IR signal. Thanks to this first understanding, the Darcian permeability is linked to the observed IR signal. A linear regression is proposed with the peak width which is judged to be the most relevant parameter. Finally, an analytical approach is developed to fit ordinary differential equations to IR peak measures and to correlate the parameters of the law to the Darcian permeability. Several laws (linear, logarithmic and power) are proposed depending on the parameter but the linear regression involving the coefficient noted β_1 is the most promising. One of the advantages of this method is to be able measuring the permeability during the flight and not only on-ground with specific test facility.

Keywords Darcy · Infrared spectrometry · Porous material · Permeation determination · Active cooling

List of symbols

K_D	Darcian permeability (m^2)
K_F	Forchheimer permeability (m)
L	Porous media thickness (m)
P	Pressure (Pa)
Q	Flow rate ($m^3\ s^{-1}$)
T	Time (s)
v	Fluid velocity ($m\ s^{-1}$)
V	Volume (m^3)
X	Mole fraction ()
α	Adjustment coefficient
β	Adjustment coefficient
μ	Dynamic viscosity (Pa.s)
ΔP	Pressure drop through the porous material (Inlet Pressure minus outlet one, in Pa)
ρ	Density ($kg\ m^{-3}$)
0	Subscript for initial conditions (time t=0)

N. Gascoin (✉) · G. Fau · P. Gillard
University of Orléans, 63, Avenue de Lattre de Tassigny, 18000 Bourges, France
e-mail: Nicolas.Gascoin@bourges.univ-orleans.fr

G. Fau
e-mail: gfau@bourges.univ-orleans.fr

P. Gillard
e-mail: pgillard@bourges.univ-orleans.fr

Published online: 17 May 2011

Bench Subscript for the bench outlet
Cell Subscript for FTIR (Fourier Transform Infra Red spectrometer) optical cell
Inlet Subscript referring to inlet conditions of the cell or of the bench

1 Introduction

The determination of permeation parameters is of prior importance for porous structures to estimate their cooling efficiency [1]. Numerical work is the preferable way to predict the multiphase flow behaviour with heat transfer, which is particularly difficult at experiments [2]. Computational Fluid Dynamics software still present average success in the right prediction of flow field in complex porous media, such as in Ceramic Matrix Composite materials. This is due to multi-layer conception and heterogeneity. The use of experiments under extreme temperature and pressure conditions is difficult for several reasons (in addition to technical problems of tightness seal notably at high temperature). First, the permeation parameters should depend on the material only. Nevertheless, due to the heterogeneity of structures after the manufacturing process, large discrepancies can be found between two samples which should present exactly the same properties. This is independent from the test reproducibility [3]. Second, when the test temperature is increased, the thermal gradients in the porous sample are difficult to manage and to monitor. Thermal heterogeneity can also be encountered between the fluid and the solid [4]. Consequently, the conditions may not be controlled perfectly at the experiments which impacts on the permeation data. Third, global laws instead of inapplicable 3-D ones (supplementary source of uncertainty due to this simplification) are used with intermediate coefficients and properties such as the dynamic viscosity and density. The variation of these latest through the porous media due to pressure drop and to the thermal gradient are very difficult to consider despite some work to improve this point [5].

Consequently, numerical simulations should be preferred to investigate multi-physics reacting flow in permeable materials, particularly to manage a full 3-D case. The codes rely on the permeability data and for this reason, experimental work remains the first step. Knowing the permeability of the material under "real" conditions is important and moreover, knowing it during the application would be of larger benefit. No method currently exists to determine the permeability of a structure, especially under high speed flight conditions. For example, the combustion chamber of SCRamjet engine is expected to be cooled directly by the fuel which filtrates through the porous wall (internal convection, film cooling and endothermic pyrolysis) [1–5]. Due to reacting process (pyrolysis coupled to heat and mass transfer), to coke formation and to degradation of the composite structure itself, the permeability is expected to change strongly (several orders of magnitude) [6]. Since this permeability controls the cooling efficiency, it is necessary to monitor its variation in real-time and in situ. The Infra red technique is known to be usable onboard of such engine [7].

Consequently, instead of using mass flow and associated pressure drop to determine the Darcian term, this paper proposes a novel experimental approach to contend with some of the related problems. The use of intermediate calculated viscosity and density is avoided. The knowledge acquired from chemical reactor engineering will be applied and this makes this study to be a transverse work between two scientific communities. In chemical and petrochemical plants, the time distribution characterization of the process is required because the phenomena highly depend on the temperature and time (steam cracking, coke formation) [8, 9]. The Fourier Transform Infra Red spectroscopy is judged to be a feasible way to determine the permeation parameters by using the Infra-Red signal modification of a tracer between the inlet and outlet of the porous media [3]. This is the framework of this study.

Several types of flow in open chemical reactor can be observed, from the ideal piston (same residence time for all the molecule natures) to the perfectly stirred reactor (no specific residence time) [10]. Some stationary incompressible models are available to consider the Residence Time Distribution (RTD). This phenomenon accounts for the modification of inlet tracer signal inside a reactor by observing the resulting outlet tracer signal. Other parameters can be considered such as the "inner age" (elapsed time of the molecule inside the reactor since injection) and "life time" (remaining time before exit of the molecule) whose sum gives the residence time [11]. The RTD is probably the most interesting parameter [12] because it allows accessing a transfer function to convert an inlet signal into an outlet one through a convolution product [11]. Finding fundamental description of this transfer function would be of great benefit to model the fluid flow through porous media.

The RTD analysis is often conducted for incompressible flow at ambient conditions but supercritical inert fluids (H_2O and CO_2) have also been studied [13, 14]. These works involved experimental and analytical work on the basis of partial differential equation [14]. The tracer is often measured by Ultra Violet and visible spectrometer [13, 14]. The resulting discrepancies of the analytical model often reach 100–200% due to the simplicity of models compared to transient flow behaviour. Furthermore, in case of multi-phase and multi-species flow, the molecular diffusion should notably be taken into account [15].

To our knowledge, no permeation model exists in relationship to the RTD. Rodier et al. [16] studied filtration process but no clear consideration was done for the Darcian and Forchheimer terms. Habisreuther et al. [10] also studied flow in open foams but they developed full 3D CFD strategy to reproduce the RTD and pressure drop numerically. Consequently, to our knowledge, this is the first time such analytical work is developed.

2 Materials and methods

The COMPARER test bench [17], used with specific cell for porous media, is briefly presented in Sect. 2.1 with the acquisition parameters of the FTIR apparatus. More details are provided in Sect. 2.2 on the ordinary differential equation used for the analytical work, which aims at linking the optical parameters to the permeation ones.

2.1 Experimental bench

It is composed of nitrogen supply system connected to the inlet of the process (Fig. 1a). The inlet pressure is fixed and the mass flow rate is imposed by singular and regular pressure losses of the bench composed of tubes, sensors and -most of all- of the permeation cell in which the porous media is inserted (Fig. 1b). By controlling the inlet pressure, several mass flow rates can be achieved and these results are generally used [3] to provide Darcian and Forchheimer permeability through the Eq. 1. Nevertheless, this methodology is not the one retained for the present work because it is preferred to observe the Infra Red signal modification of a tracer through the porous media. The permeable materials which are considered in this study are metallic samples in stainless steel (30 mm of diameter, 3 mm of thickness) of class 3 and class 40 (Poral materials manufactured by Federal Mogul). More details on these samples can be found in [3]. They have been selected because they are well characterised (grain diameter, pore diameter, porosity, permeability) and isotropic. The SS40 (1.81×10^{-11} m^2 and 40% of porosity) presents higher porosity, thus higher permeability, than SS3 (typically 1.92×10^{-13} m^2 and 30%).

$$\frac{\Delta P}{L} = \mu . \frac{v}{K_D} + \rho . \frac{v^2}{K_F} \quad (1)$$

In addition to this configuration (more details can be found in [3]), a small tank of tracer is placed upstream the process (in parallel to the nitrogen supply line). Downstream, a sampling line is used to collect part of the main flow. It is connected to an optical cell in which the IR measures are conducted with a FTIR spectrometer (Nicholet). It would have been preferred to connect the optical cell directly to the process outlet but the tracer quantification method has been developed for absolute pressures of 50 mbar [18]. This pressure is regulated thanks to a vacuum pump which is not able to manage high mass flow rate (required to get permeation data in conditions of interest). The residence time in the process is about 0.7 s for a mass flow rate of 0.048 g s^{-1} and about 10 s at 0.0031 g s^{-1}. It is roughly constant in the sampling line at about 1.8 s. The one in the optical cell has been estimated in previous study [18]. It is contained between 140 and 280 s. During the tracer injection, the residence time decreases due to the mass flow rate increase. The nitrogen is chosen as reference for the carrier gas (main flow) because it is not seen by IR and the methane is the standard tracer for opposite reason. Some tests to be presented in Sect. 3.2 have also been conducted with mixture of nitrogen and methane to observe the diffusion of hydrogen in porous media notably (decrease of the methane signal).

The FTIR spectrometer signal is acquired with specific data acquisition system (not the same as other sensors which are acquired with two other data acquisition system). This implies three different time bases which are homogenised with an uncertainty of 1–2 s. The acquisition range of FTIR (3,050–3,150 cm^{-1}) corresponds to the

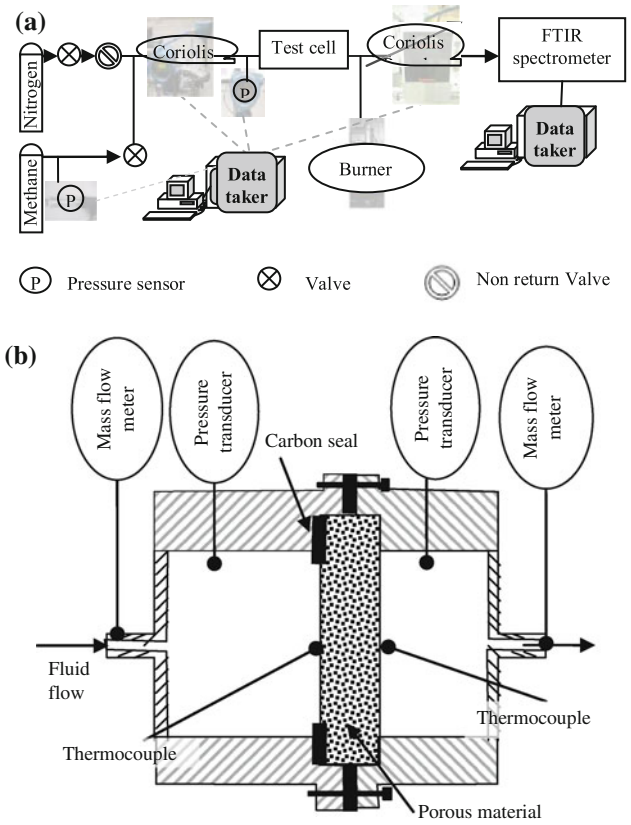

Fig. 1 Experimental bench for analysis of a tracer in a gas flow (**a**) through porous media inserted in specific cell (**b**)

rotation-vibration of methane. It is quite narrow to enhance the acquisition frequency. More information about internal FTIR adjustments can be found in Ref [18]. The following setups are chosen:

- Number of scans for each spectrum: 1
- Resolution: 4 cm^{-1}
- Acquisition range: 3,050–3,150 cm^{-1}
- Background acquisition (64 scans) before the measure of sample
- Detector: DTGS (Deuterated TriGlycide Sulfate)
- Beam splitter: KBr
- Moving speed of the mirror: about 0.48 cm s^{-1}
- Numerical gain: 8

The tests are conducted as follows. First no porous sample is placed in the cell to understand the relationship between optical and physical parameters (mass flow, pressure). Secondly, a permeable media is considered to link the optical parameters to permeation data (Darcian term). A constant N_2 flow is delivered with a fixed inlet pressure and a small volume of methane (about 40 cm^3) is periodically injected in the main flow with a fixed gauge pressure. To deliver the tracer, a manual valve is open and then closed rapidly (about 0.5 s of opening time). The signal is modified from the upstream injection to the optical cell because of transport in the main process and also in the sampling line to the FTIR. The modification of the signal must be understood (next section) as a function of the following parameters:

- Main flow rate of carrier gas
- Sampling line flow rate
- Nature of carrier gas and of tracer
- Injected quantity of tracer
- Permeation of the bench (porous media)

2.2 Analytical exploitation and formulas

The IR signal modification is expected to be done by two successive steps of transport in the bench and in the sampling line (Fig. 2). The first peak corresponds to the injection when the valve is commuted to inject the tracer in the main flow. This signal should be a well-strobe marker (infinite value for rising and falling gradients) but it is probably not ideal due to the opening and closing time and due to non-constant pressure or mass flow rate tracer supply. Nevertheless, the developed analytical method should takes this point into account and some successive experimental preliminary tests aim at approaching it. The second peak is obtained in the process after the transport and diffusion of the well-strobe marker along the reactor. It can be assumed that, as it is observed in classical chemical analysis such as Gas Chromatography, the time derivative of rising and falling gradients will be finite (Fig. 2). The peak width will be larger while the peak height will be lower to ensure the peak surface conservation. A time delay, indexed 1, is found (Fig. 2). The modification of the injection signal is the first step of the analytical work. This is an essential study in chemical reactor characterisation. A perfect or ideal reactor should transmit the signal without perturbation but this is rarely observed.

The second step consists in the same modification but it is probably more difficult to analyse because this is related to the sampling of the main flow towards a line with lower mass flow rate than the carrier gas. If this flow rate is too low, the sampling is not representative of the process and the signal can be lost because of a dilution effect. If this flow rate is high enough, the signal can be representative. However, it is of smaller magnitude because only a small part of the main flow is analysed (Fig. 2). The peak surface is not equal to the inlet upstream signal.

To conduct the analytical work on the basis of the first results and to understand the optical/physical parameters relationship, the classical ordinary differential equation of the concentration in a renewed volume is considered (Eq. 2). It is based on mass balance inside the volume of study. The mole fraction is assumed to be homogeneous in the volume and it is expressed as a function of the volume of the cell and of the related volume flow rate. Eq. 2 is considered with the corresponding solution (Eq. 3). The flow rate Q_{cell} can be determined experimentally but the inlet mole fraction X_{inlet} remains unknown. Consequently, the primary task is to determine X_{inlet} on the basis of experimental measures. It is expected to be able describing the mass transfer phenomena in the system thanks to this Eq. 2, which is applied two times for the bench and for the sampling line.

$$\frac{dX_{cell}(t)}{dt} = \frac{Q_{cell}(t)X_{inlet}(t)}{V_{cell}} - \frac{Q_{cell}(t)X_{cell}(t)}{V_{cell}} \tag{2}$$

$$X_{cell}(t) = e^{-\int_0^t \frac{Q_{cell}(x)}{V_{cell}}dx}\left(X_0 + \int_0^t \frac{Q_{cell}(x)X_{inlet}(x)}{V_{cell}} e^{\int_0^x \frac{Q_{cell}(u)}{V_{cell}}du}dx\right) \tag{3}$$

with X_{cell} the molar fraction of the considered species in the cell which should be measured by the FTIR, X_{inlet} the

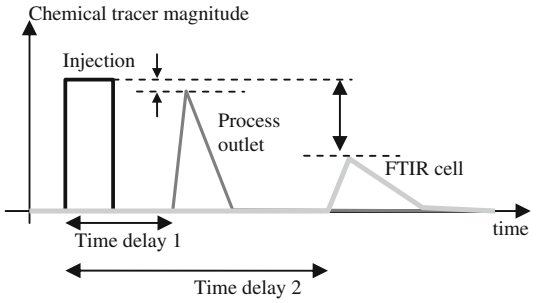

Fig. 2 Theoretical modification of the upstream tracer signal along the experiment and up to the FTIR cell

incoming molar fraction of the considered species (the tracer) at the inlet of the cell, Q_{cell} the volume flow rate in the cell and V_{cell} the volume of the cell. Of course, the "cell" subscript can refer to the bench or to the FTIR volume to investigate both phases of the tracer signal modification.

The analytical Eq. 3 is then modified (Eqs. 4 and 5) to enable adjusting the analytical estimation onto the experimental data if necessary. For this purpose, some coefficients are introduced and the final aim is to link them with the Darcian permeability. It is also wanted to propose physical meaning of these coefficients to extend this simple approach to a wider field of study. The Eq. 4 is used to model the signal modification through the test bench and the Eq. 5 to model the one through the FTIR optical cell. The parameters α_i, β_i which are added in the analytical model will be adjusted empirically. To do so, the FTIR estimated signal (expressed in terms of mole fraction) will be compared to the FTIR measured signal (in term of absorbance). It would be required to have a quantitative analysis of the measured FTIR signal to express it in tracer mole fraction. For this purpose, the quantitative IR method of the PRISME institute could be used [18]. Nevertheless, it is not adapted to the present FTIR parameters because the current settings are chosen for a high acquisition frequency instead of high signal quality.

It can be noticed that the two coefficients α_i, β_i are linked if they do not depend on the time. The sampling line flow rate is 5.56 ml s^{-1}, with a sampling line plus optical cell volume of 110 cm^3. The bench volume is 26 cm^3 (the test cell has a volume of 14.6 cm^3) and the process flow rate is the measured transient one. A very short study enabled to understand the impact of flow rate or cell volume on the analytical FTIR signal. It can be concluded that increasing the sampling line flow rate gives a higher magnitude of the FTIR estimated signal and a lower peak width.

$$X_{bench}(t) = e^{-\alpha_1 \int_0^t \frac{Q_{bench}(x)}{V_{bench}} dx} \left(X_0 + \int_0^t \frac{Q_{bench}(x) X_{inlet}(x)}{V_{bench}} e^{\int_0^x \beta_1 \frac{Q_{bench}(u)}{V_{bench}} du} dx \right) \quad (4)$$

$$X_{cell}(t) = e^{-\alpha_2 \int_0^t \frac{Q_{cell}(x)}{V_{cell}} dx} \left(X_0 + \int_0^t \frac{Q_{cell}(x) X_{inlet}(x)}{V_{cell}} e^{\int_0^x \beta_2 \frac{Q_{cell}(u)}{V_{cell}} du} dx \right) \quad (5)$$

with α_i, β_i are tabulated parameters and where $i = 1$ in the bench and 2 in the optical cell.

3 Results and discussion

The tests have been first conducted without porous media to observe the variation of the IR signal as a function of test parameters. Then, porous media has been inserted in the test cell to determine the impact of permeability on the signal modification. A design of experiment allowed providing quantitative estimation of the effect of each physical parameter on the optical IR peak (Sect. 3.1). Thanks to this work, relationships between parameters are presented to find some analytical laws linking the measures to the intrinsic permeation properties (Sect. 3.2).

As a preliminary work, the reproducibility of the tests was first verified, notably to ensure the correct tracer injection through the manual valve opening (Fig. 3a). The overall low variance shows the good reproducibility of the tests. The absorbance signal in the range of 3,050–3,150 cm^{-1} (Fig. 3b) obtained by FTIR is aimed to be correlated to injection parameters.

The variations of physical parameters are correlated to optical modifications. Considering some test results with and without porous media (Fig. 4), the overpressure (due to tracer injection) and mass flow rate which are measured during the test have been monitored for two input carrier gas mass flow rates (50 and 100 mg s^{-1}). The pressure signal (Fig. 4a, c) is quite dependent on the system permeability because of the "fixed" mass flow rate and of the downstream pressure which is equal to the atmosphere. The mass flow rate (Fig. 4a, c, respectively 50 and 10 mg s^{-1}) also impacts the overpressure. The time needed to evacuate the overpressure (Fig. 4a) is lower for a class 3 sample (about 6.5 s at 50 mg s^{-1}) than for class 40 or for no sample (about 9 s at 50 mg s^{-1}) probably because the overpressure is lower. At 100 mg s^{-1} (Fig. 4c), the overpressure is also lower for low permeability class porous sample but the time needed to evacuate this pressure is longer (9 s for class 3 and 12 s for class 40 or for no sample with similar overpressure value). The mass flow rate which is measured for the 50 mg s^{-1} test case during the injection (Fig. 4b) is not very different between the class 3 and 40 samples. At 100 mg s^{-1} (Fig. 4d), the mass flow rate does not significantly increase for the class 3 sample (the two extreme values –gain and loss of mass- may be attributed to mass flow rate sensor variation). The mass flow rate of carrier gas (main flow) and the pressure are probably the most important physical parameters and a design of experiment is proposed in the next section to confirm it. It can be noted that the acquisition frequency is underdefined compared to the high dynamic of the physical parameters because the number of points describing the peak of mass flow (Fig. 4b) is low, particularly for the empty cell. As a consequence, the signal may be underestimated. Nevertheless, at least qualitatively, the overpressure acts in the same way as the mass flow rate increase (Fig. 4a, b).

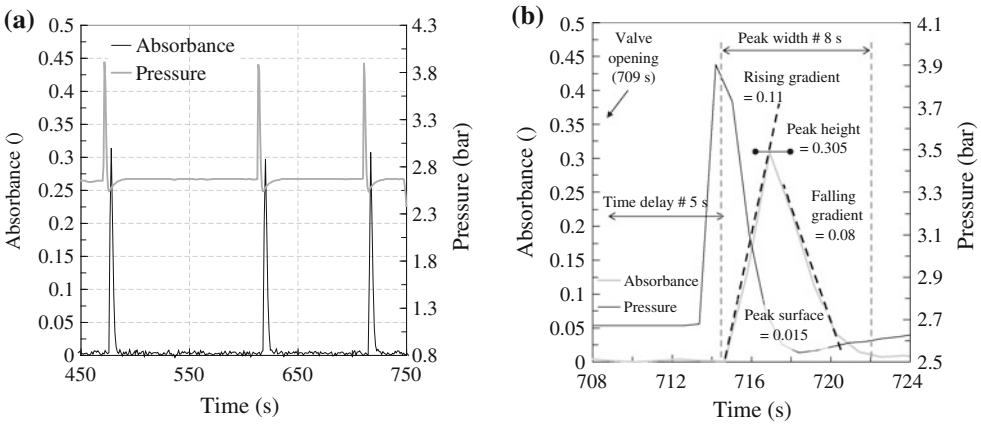

Fig. 3 Reproducibility of three successive tests (**a**) and details of peak analysis on the third peak for the test numbered three (**b**)

3.1 Design of experiment

Different test conditions with several natures of fluid (tracer and carrier gas), mass flow rate and tracer quantities have been considered within a test matrix to observe possible interactions (Table 1). The optical FTIR signal results are given for analysis of the parameters effect. The peak height is given without unit because this is the absorbance of the signal, which is a dimensionless parameter. The injected mass of tracer accounts for the pressure effect (as it was presented in previous section). This mass is estimated by the difference of pressure before and after injection. The characteristics of the tests are summarized in Table 2. Thanks to the effects of physical parameters (Table 1), the Darcian permeability, the injected tracer mass and the main flow rate (so as to their interactions) –in this order of importance- are found to play a role on the time delay (Fig. 5a). All the parameters seem to impact the peak height (Fig. 5b) but the permeability impacts it in the opposite way of the others (Table 1). Its effect is of the same order than the sampling line flow rate in absolute value (Table 1). The diagram of peak width (Fig. 5c) shows the major role of the permeability. The effective diagram of the rising gradient is strictly the opposite of the falling gradient one. This latest is very similar to the one of peak height (Fig. 5b).

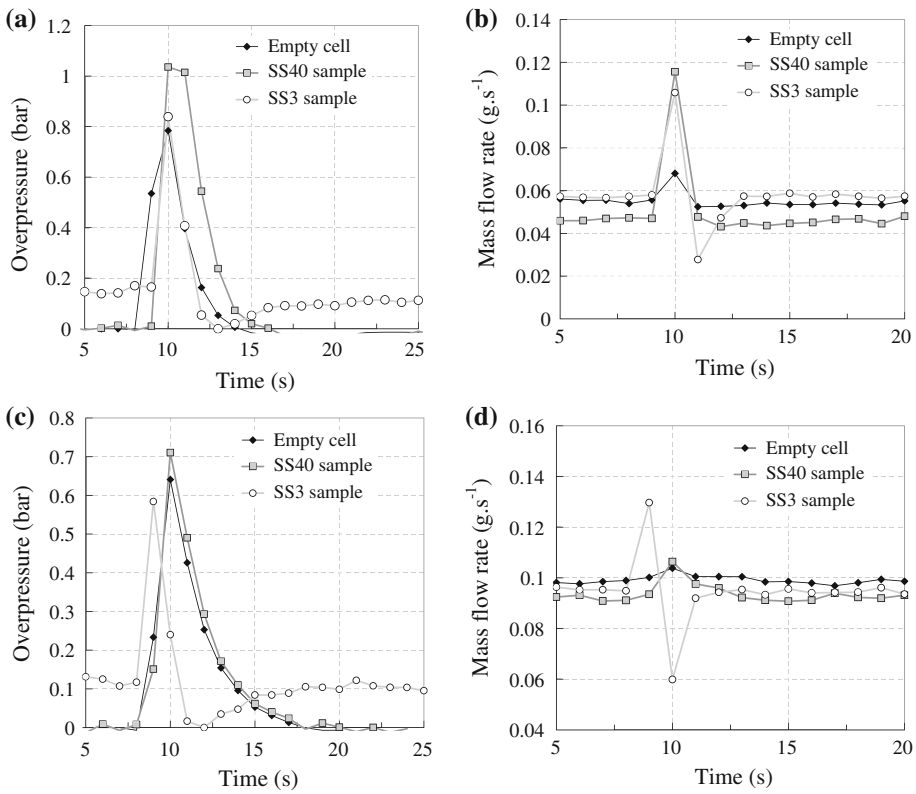

Fig. 4 Overpressure (**a**, **c**) and mass flow rate (**b**, **d**) measured during test of different porous media at 50 mg s^{-1} (**a**, **b**) and 100 mg s^{-1} (**c**, **d**)

Table 1 Design of experiment to estimate quantitatively the effects of the physical parameters on optical ones

		A	B	C	D	AB	AC	AD	BC	BD	CD					
		Physical test parameters				Interactions						Optical results				
		Main flow rate (g/s)	Sampling line flow rate (l/s)	Injected quantity (g)	"Darcian permeability" of the bench (m^2)	AB	AC	AD	BC	BD	CD	Time delay (s)	Peak height ()	Peak width (s)	Raising gradient (s)	Falling gradient (s)
First campaign	Test n°1	−1	−1	−1	1	1	1	−1	1	−1	−1	3.2	0313	6.1	0.1367	−0.0904
	Test n°2	−1	−1	−1	1	1	1	−1	1	−1	−1	2.2	0.415	21.2	0.1643	−0.0330
	Test n°3	−1	−1	−1	1	1	1	−1	1	−1	−1	1.8	0.445	26.3	0.1707	−0.0302
Second campaign	Test n°4	−1	−1	1	1	1	−1	−1	−1	−1	1	21.5	0046	115.5	0.0023	−0.0010
	Test n°5	1	−1	1	1	−1	1	1	−1	−1	1	18.3	0045	93.0	0.0034	−0.001
	Test n°6	1	−1	1	1	−1	1	1	−1	−1	1	18.7	0034	65.0	0.0032	−0.001
	Test n°7	1	−1	1	1	−1	1	1	−1	−1	1	18.7	0020	38.7	0.0021	−0.001
Cell	Test n°8	−1	1	1	1	−1	−1	−1	1	1	1	1.9	0071	10.3	0.0392	−0.0117
	Test n°9	1	1	−1	1	1	−1	1	−1	1	−1	1.7	0042	8.7	0.0142	−0.0073
Class 3	Test n°10	−1	1	1	−1	−1	−1	1	1	−1	−1	2.9	0058	10.0	0.0139	−0.0091
	Test n°ll	1	1	−1	−1	1	−1	−1	−1	−1	1	4.1	0055	9.0	0.0191	−0.0093
Class 40	Test n°12	−1	1	−1	1	−1	1	−1	−1	1	−1	3.3	0070	11.0	0.0252	−0.0094
	Test n°13	1	1	−1	1	1	−1	1	−1	1	−1	4.2	0049	8.0	0.0266	−0.0074
Cell	Test n°14	−1	1	1	1	−1	−1	−1	1	1	1	3.6	−0.140	7.2	0.0274	0.0274
Cell	Test n°15	−1	1	−1	1	−1	1	−1	−1	1	−1	2.6	−0.142	6.2	0.0198	0.0198
	Time delay (s)	1.5	−4.0	4.2	6.3	−2.1	1.9	1.4	−5.2	−4.9	4.3	7.2	0.092	29.1	0.0445	−0.0110
	Peak height ()	−0.060	−0.084	−0.074	0.077	0.090	0.068	−0.059	0.063	−0.99	−0.075					
	Peak width (s)	0.6	−19.7	16.2	26.5	−3.1	6.6	0.7	−18.3	−22.2	16.1					
	Raising gradient (s)	−0.0354	−0.0198	−0.0323	0.0402	0.0267	0.0255	−0.0361	0.0291	−0.0242	−0.0317					
	Falling gradient (s)	0.0074	0.0100	0.0113	−0.0085	−0.0128	−0.0085	0.0074	−0.0086	0.0125	0.0113					

Table 2 Dependency of FTIR signal characteristics on test characteristics (of CH_4 around 3,000 cm^{-1})

		Physical test parameters							Optical results					
		Main flow rate (g/s)	Sampling line flow rate (1/s)	FTIRcell volume (m^3)	Bench volume (m^3)	Carrier gas molecular weight (g/mol)	Tracer molecular weight (g/mol)	Injected quantity (s)	''Darcian Permeability'' of the bench (m^2)	Time delay(s)	Peak height ()	Peak width (s)	Raising gradient (s)	Falling gradient (s)
First campaign	Test n°l	0.043	0.0056	l.E-04	2.6E-05	28	16	0.0887	5.00E-12	32	0.313	6.1	0.1367	−0.0904
	Test n°2	0.004	0.0056	l.E-04	2.6E-05	2 g	16	0.1035	5.00E-12	22	0.415	21.2	0.1643	−0.0330
	Test n°3	0.003	0.0056	l.E-04	2.6E-05	2 g	16	0.1339	5.00E-12	12	0.445	26.3	0.1707	−0.0302
Second campaign	Test n°4	0.050	0.0006	l.E-04	41E-05	28	16	0.4664	5.00E-12	21.5	0.046	115.5	0.0023	−0.0010
	Test n°5	0.079	0.0006	l.E-04	41E-05	28	16	0.5039	5.00E-12	18.3	0.045	93.0	0.0034	−0.001
	Test n°6	0.115	0.0006	l.E-04	41E-05	28	16	0.4420	5.00E-12	18.7	0.034	65.0	0.0032	−0.001
	Test n°7	0.124	0.0006	l.E-04	41E-05	28	16	0.3844	5.00E-12	18.7	0.020	38.7	0.0021	−0.001
Empty cell	Test n°8	0.050	0.3611	l.E-04	41E-05	28	16	0.2025	1.31E-12	19	0.071	10.3	0.0392	−0.0117
	Test n°9	0.100	0.3611	l.E-04	41E-05	28	16	0.1436	1.31E-12	1.7	0.042	8.7	0.0142	−0.0073
Class 3	Test n°10	0.050	0.3611	l.E-04	41E-05	28	16	0.2489	1.92E-13	29	0.058	10.0	0.0139	−0.0091
	Test n°ll	0.100	0.3611	l.E-04	41E-05	28	16	0.1539	1.92E-13	4.1	0.055	90	0.0191	−0.0093
Class 4	Test n°12	0.050	0.3611	l.E-04	41E-05	28	16	0.1988	1.81E-11	33	0.070	11.0	0.0252	−0.0094
	Test n°13	0.100	0.3611	l.E-04	41E-05	28	16	0.1736	1.81E-11	42	0.049	8.0	0.0266	−0.0074
Empty cell	Test n°14	0.050	0.3611	l.E-04	41E-05	22	28	0.3525	1.31E-12	36	−0.140	7.2	0.0274	0.0274
Empty cell	Test n°15	0.050	0.3611	l.E-04	41E-05	22	2	0.0391	1.31E-12	26	−0.142	6.2	0.0198	0.0198

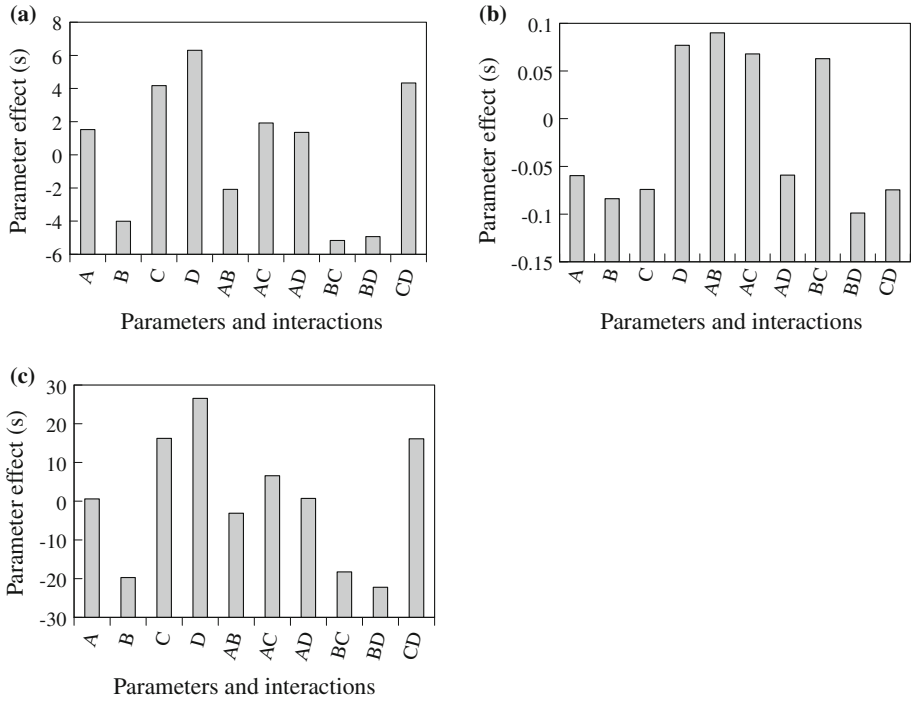

Fig. 5 Effects diagram of parameters on time delay (**a**) and on peak height (**b**) and width (**c**)

Table 3 Qualitative relationships between operating conditions and FTIR infrared signal

Optical results	Physical test parameters							
	Main flow rate (g/s)	Sampling line flow rate (1/s)	FTIR cell volume (m^3)	Bench volume (m^3)	Carrier gas molecular weight (g/mol)	Tracer molecular weight (g/mol)	Injected quantity (g)	"Permeation" of the bench
Time delay (s)	+(↔)	+(↓)	o(↑)	o(↑)	?	+(↑)	?	?
Peak height (s)	+(↓)	+(↑)	o(↓)	o(↓)	+(↑)		+(↑)	+(↓)
Peak width (s)	+(↓)	+(↓)	o(↑)	o(↑)	?	?	+(↑)	o(↑↓)
Rising gradient (s)	+(↓)	+(↑)	o(↓)	o(↓)	+(↑)	+(↔)	?	?
Falling gradient (s)	+(↓)	+(↑)	o(↓)	o(↓)	?	+(↔)	+(↑)	?

The sign "−" signifies that no correlation has been shown the sign "+" signifies that a correlation has been shown the sign "o" signifies that no clear conclusion has been a dressed the sign "?" signifies that this correlation has not been elucidated the signs | or | indicate an increase or a decrease of the optical parameter in case of an increase of the physical one

Finally, it would be easier to study the permeation through the analysis of the peak width. The relative difference between parameters is lower than for the time delay but the peak width is easier to measure due to possible automation, due to higher value—thus lower uncertainty—and because the exploitation of a time signal needs a good synchronisation of the acquisitions (which is difficult with three different systems).

Qualitatively (Table 3), the carrier gas flow rate, when increased, decreases the rising gradient, the peak width, the height and the surface. The sampling line flow rate, when increased, increases the rising and falling gradients and the peak height but it decreases the peak surface, the peak width and the time delay. The tracer molar mass, when augmented, increases the time delay. The valve opening time of the tracer tank, when enlarged, decreases the falling gradient by a rise of the decreasing time (linked to the falling gradient). The injected mass of tracer, with coupled effect of carrier gas flow rate, when increased, increases the peak width, its height, its surface and the rising gradient but it decreases the falling gradient. These qualitative observations are important to understand the relationships between parameters.

3.2 Relationships between optical and physical parameters

The quantitative approach is necessary to provide permeability estimation. Some relationships have been searched between the characteristics of the FTIR peak and the bench configuration or test conditions. The FTIR peak width corresponds to the duration of the FTIR signal

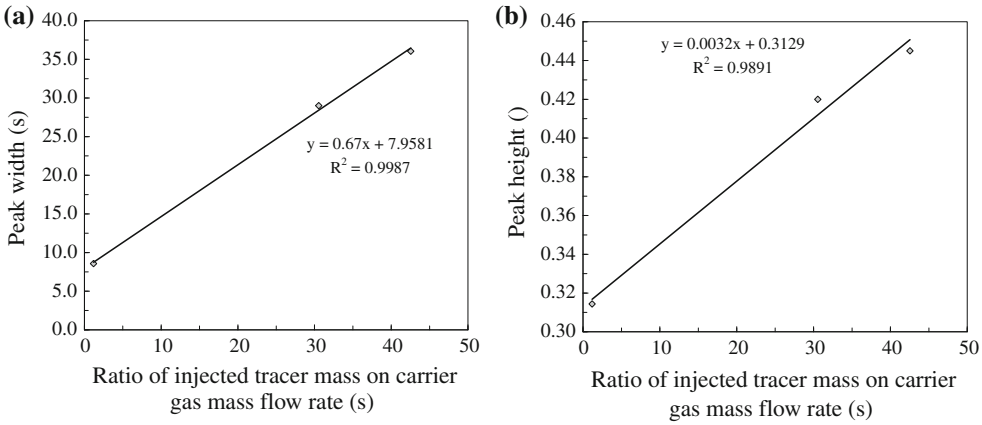

Fig. 6 Peak width (**a**) and height (**b**) as a function of tracer and carrier gas flow

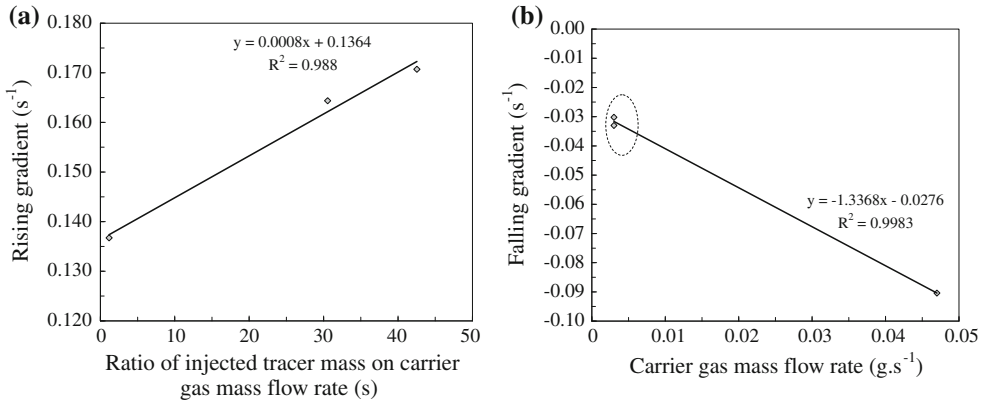

Fig. 7 Effect of the tracer and/or carrier gas flow rate on the rising gradient (**a**) or falling one (**b**)

measurement, i.e. the time during which methane flows in the optical cell. It depends firstly on the carrier gas flow rate (the higher the flow rate the lower the peak width) and secondly on the injected tracer quantity (the higher the injected quantity, the higher the peak width). This is illustrated by Fig. 6a. Of course, the sampling line flow rate impacts on this value (Table 3). The peak height corresponds to the maximum absorbance (Fig. 6b). It is linked to the ratio of the tracer flow rate on the carrier gas one. As a consequence of these two FTIR peak characteristics, the peak surface depends on the injected mass and carrier gas flow rate. A synchronisation effect between the main flow and the sampling line flow may also exist.

The delay between the valve opening and the FTIR signal apparition (the so-called detection time delay) is roughly constant whatever the carrier gas flow rate (in regard to the lack of synchronisation between the three acquisition systems). This shows that the process has a minor impact on this point and consequently, that the time delay is driven by the chemical diffusion. The increase of the sampling line flow rate decreases the time delay.

The time-derivative of the increasing FTIR signal (the so-called rising gradient) is mainly linked to the ratio of tracer injected mass on the carrier gas mass flow rate (Fig. 7a). It decreases with the decrease of carrier gas flow rate. The time-derivative of the decreasing signal

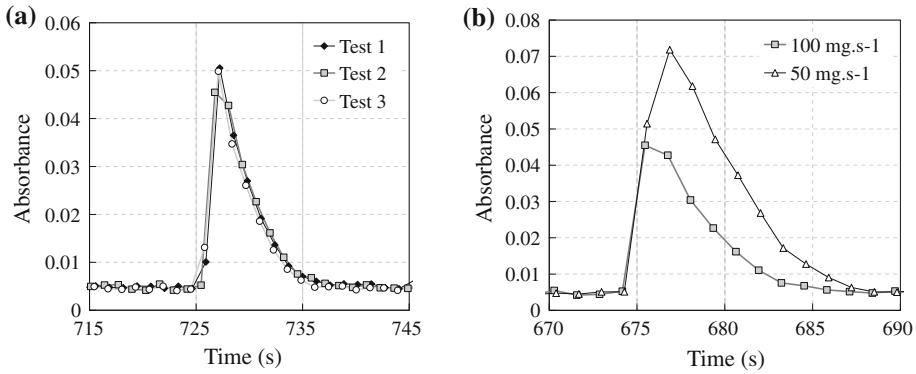

Fig. 8 Example of reproducibility of tests at 100 mg s^{-1} through SS40 sample (**a**) and influence of the mass flow rate for tests with SS40 sample (**b**)

(the so-called falling gradient) can also be observed (Fig. 7b). It is not dependent on the injected tracer quantity. It decreases with the carrier gas flow rate (the dynamic is slowed down). For approximately the same carrier gas flow rate, two points have not exactly the same gradient value (Fig. 7b). This is attributed to the conditions of the test because the last test configuration corresponds to a valve opening time of 3 s. Consequently, the tracer which remains in the volume after injection of the second test condition is evacuated slowly by a kind of venting effect when the carrier gas flows. As a result, the peak width is somewhat greater and the falling gradient is lower, which means the decreasing time of the peak is longer. The falling gradient is also impacted by the sampling line mass flow rate and by the injected tracer mass. The analytical model should verify that a decrease of this sampling flow should be accompanied by the one of the peak height and of the two time-derivatives but also by a rise of other characteristics.

Two test series have been conducted with class 3 and 40 SS Poral samples (SS3 and SS40 respectively) with two carrier gas mass flow rates (50 and 100 mg s^{-1}). The reproducibility of each test configuration is verified (Fig. 8a). The signal measured by FTIR is lower for higher carrier gas mass flow rate (Fig. 8b). This is notably due to the dynamics of sampling which is too slow for high carrier gas flow rate. A dilution effect of sample into the process flow is responsible for the lower signal in case of higher carrier flow. As a response, the sampling flow rate should be increased to get higher signal. This flow rate plays a role with the injected mass and the carrier gas flow.

The effect of the porous sample is not obvious because it is seen through a sampling process (Fig. 9a). A "synchronisation issue" appears because for low nitrogen mass flow rate, the FTIR signal is lower in case of low permeability value (class 3 sample) while it is higher for high flow rate. The case without porous sample is judged to be the ideal case with the right timing between the main flow and the sampling flow. At 50 mg s^{-1}, the class 40 does not slow the fluid down too much and the results are very similar to those without porous sample due to the large porosity of the material. As a consequence, the optical method is shown to be more adapted to very low permeability material (K_D of 10^{-13} m^2 and less probably). At 100 mg s^{-1} (Fig. 9b), the carrier gas flows too rapidly without porous sample. With the high porosity sample (class 40), the flow is slightly slowed down and the class 3 drastically reduces the flow, which gives higher absorbance value, close to the value of the 50 mg s^{-1} tests. As a consequence for the optical method, if it is applied to large permeability material (K_D over 10^{-13} m^2), the mass flow rate should be highly increased to improve the accuracy of the method.

Some tests have been conducted with a constant mixture of methane and of nitrogen as carrier gas. The tracer is nitrogen and successively hydrogen to observe the effect of chemical diffusion for molecules with such different molecular weight. These both tracers are not visible by FTIR but they are observed through the diminution of the methane signal (Fig. 10a). The slight absorbance increase is due to the fluid compressibility. This is a transient effect. The initial FTIR background is done under nitrogen flow to clearly see the methane signal. Due to the tracer injection system (pressurised volume), the mass which is injected is higher for nitrogen than for hydrogen. The ratio is close to 9 (0.353 g of injected N_2 and 0.039 g of injected H_2) and not 14 (28 g mol^{-1} for nitrogen and 2 g mol^{-1} for hydrogen) as it would have been expected for the ratio of molar mass. This is probably due to the rapid diffusion of hydrogen compared to nitrogen. The hydrogen injection quantity is thus higher than expected (about 40 mg while 25 mg were expected). Consequently, the equivalent tracer absorbance signal (deduced from the absorbance) is higher for nitrogen than for hydrogen (Fig. 10b). For the same reason, the delay between the injection and the detection is about 40% higher for nitrogen than for hydrogen and the peak width is 17% higher for N_2 (tests numbered 14 and 15 on Table 2). The discrepancies on the rising and falling

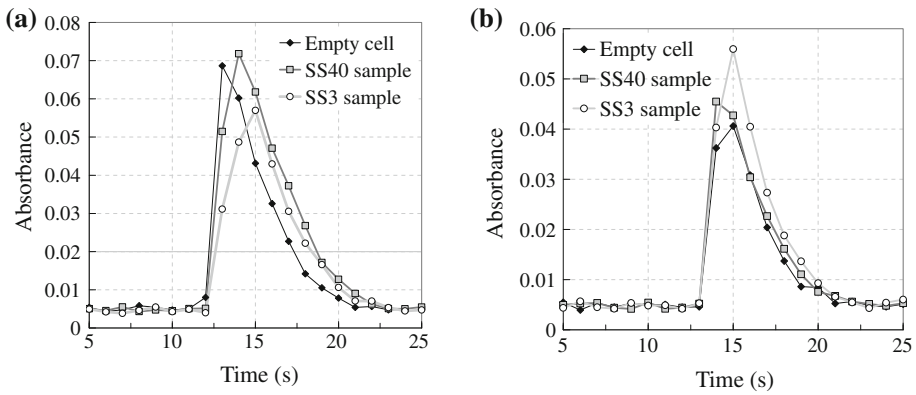

Fig. 9 Measured FTIR signal for 50 mg s^{-1} (**a**) and 100 mg s^{-1} (**b**) tests with and without porous sample

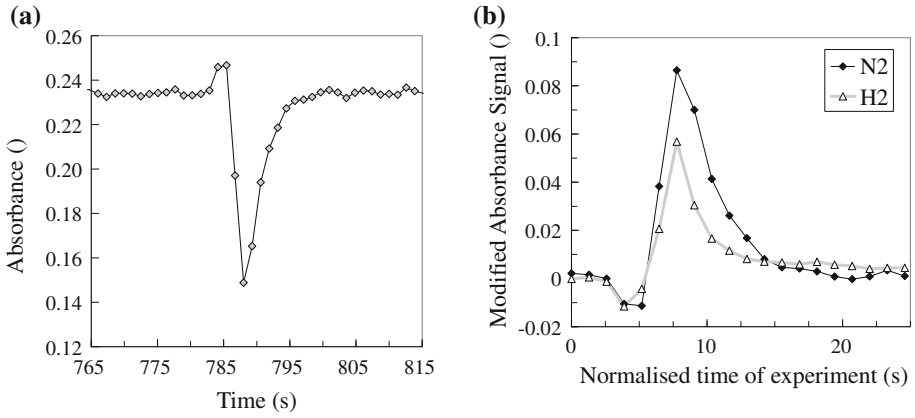

Fig. 10 Example of the methane signal decrease due to a nitrogen injection at 50 mg s^{-1} (**a**) and corresponding signal of N_2 and H_2 at 50 mg s^{-1} (**b**)

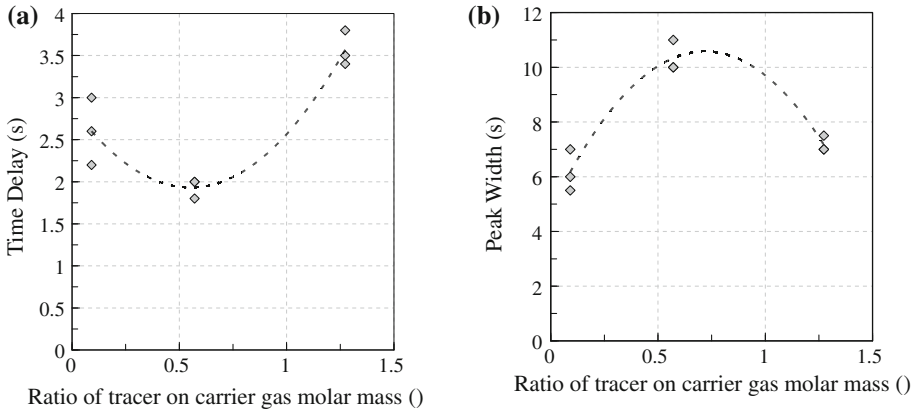

Fig. 11 Time delay (**a**) and peak width (**b**) of the FTIR signal depending on the ratio of tracer on carrier gas molecular weight

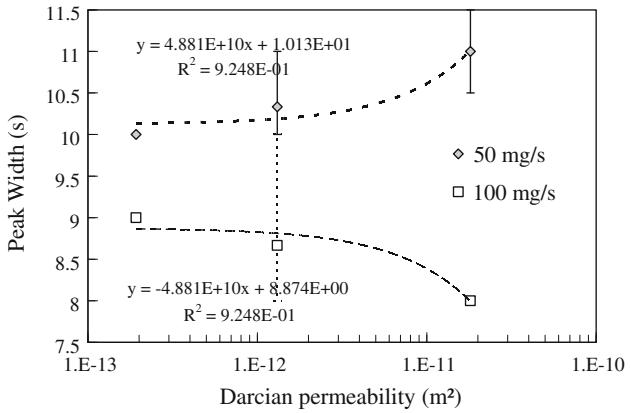

Fig. 12 Peak width of FTIR signal of tracer injection in 50 and 100 mg s^{-1} nitrogen flow

gradients are not significant. The time delay (Fig. 11a) between the tracer injection and the measure of the signal by the FTIR is linked to the main flow rate, to the sampling flow rate and to the molecular weight due to diffusion process. The peak width (Fig. 11b) and the falling gradient are also linked to these parameters. Furthermore, contrary to what could be supposed, the chemical natures of tracer and carrier gas do not impact the rising gradient. The parabolic curves (Fig. 11) seem to present maximum and minimum for a ratio close to unity which correspond to the ideal tracer.

3.3 Determination law for the Darcian permeability

On the basis of preceding section, the peak width has been judged to be the most relevant parameter to be the witness of IR signal modification by porous media. The peak width is given as a function of the Darcian term of the porous media (Fig. 12 in semi-log scale). The Darcian permeabilities are those furnished by the manufacturer of the samples. Both linear regressions give satisfying correlation factor but one is increasing and the other one is decreasing with the same director coefficient. A dilution factor and the synchronisation of the FTIR sampling method are responsible for these two trends. This highlights the relationship between optical and physical parameters. If these curves can be extended to a large number of cases, this could be a way to determine the permeability by simply measuring the peak width. For an uncertainty of 2% on the peak width determination (due to the regulation of the process and to the FTIR system uncertainty), an uncertainty of 50% is found on the Darcian term. This is higher than the one generally observed when determining the permeability (up to 30% depending on the test conditions and on the

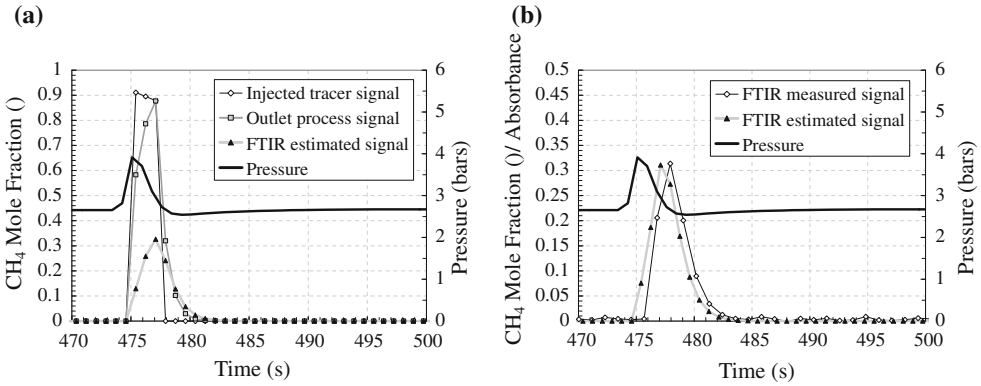

Fig. 13 IR signal modification through the bench (**a**) with comparison to experiment (**b**)

permeability level) [3]. Nevertheless, this is acceptable because this real-time in-sit quantification Infra Red method is developed for onboard application to monitor permeability variations of several orders of magnitude.

The parameters α_i, β_i (presented in Sect. 2.2) have been adjusted empirically. As an example, the test number 3 in Table 2 is observed (Fig. 13a). Eq. 4 is used to determine the so-called outlet process signal and Eq. 5 gives the so-called FTIR estimated signal. The equation coefficients are the following: $\begin{cases} \alpha_1 = 2.48 \\ \beta_1 = 2.6 \end{cases}$ and $\begin{cases} \alpha_2 = 23.9 \\ \beta_2 = 30 \end{cases}$. The determination of α_2, β_2 for the Eq. 5 is done by comparison with experimental data (Fig. 13b). The computed peak surface of the optical signal at the process outlet is 2.250 s while the one at the injection is 2.252 s (Fig. 13a). The surface conservation is satisfactory. A time delay between the two peaks lower than 1 s is observed. This is in good agreement with the residence time given in Sect. 2.2. The FTIR estimated signal surface is 0.989, which is more than two times lower than the signal at the process outlet. This is not directly linked to the flow rate of the process or sampling line due to the specific volumes and to the tabulated coefficients. The time delay between the measured and estimated FTIR signal is about 1 s (Fig. 13b) which is in the range of accuracy of the synchronisation of the three acquisition systems. It can be added that the peak width, the rising and falling gradients are also in acceptable agreement. The peak surface of the FTIR measured signal is 1.071, which is 7.7% greater than the estimated one.

It must be noted that the mathematical solution is not unique for Eqs. 4 and 5 and several couples of α_i, β_i parameters can give the same result. For the preceding example, the following set of parameters is also suitable: $\begin{cases} \alpha_1 = 20 \\ \beta_1 = 20.16 \end{cases}$ and $\begin{cases} \alpha_2 = 10 \\ \beta_2 = \end{cases}$. As a consequence, it is chosen in the following to fix the value of α_1 to 20 and of α_2 to 10 arbitrarily. The coefficients β_1 and β_2 are then adjusted as detailed above. Considering two parameters α_i, β_i in the Eqs. 4 and 5 was justified by physical considerations (diffusion of species in the flow and in the porous media). Mathematically, the α_i coefficients act on the height of the signal and on its shape while the β_i coefficients act mainly on the height of the signal. For a first step, adjusting a single coefficient is preferable.

The same work has been carried out for the other test series but the agreement is not satisfactory for a number of cases due to the difficulty to fit the peak width and peak height simultaneously. Nevertheless, satisfactory results are obtained for some cases given in Table 4 for materials SS3 and SS40. Due to the link between the coefficients α_i, β_i, one of them is fixed and the other only is varied. The range of variation remains very small for β_1 and consequently the impact on the uncertainty on Darcian term determination is large. The correlations are judged satisfactory, which is quite evident because the parameters are adjusted to minimize them. These four parameters are then related to physical data. The parameter β_1 is the most relevant parameter. A relationship is proposed with the Darcian permeability furnished by the manufacturer (Fig. 14a) and to the carrier gas flow rate (Fig. 14b). The Fig. 14a confirms the feasibility of determining the permeation properties of a porous media by means of Infrared device. The associated post-processing work is still not negligible and it is quite complex. For future onboard aerospace application, this methodology should be used to determine the Darcian permeability on the basis of real-time in situ Infra Red acquisition. After a post-processing step fitting the acquired signal by analytical equation to determine the beta coefficient, the permeability will be estimated through the proposed relationship for example (Fig. 14a).

4 Conclusion

To manage the cooling of aerospace hot structures in case of hypersonic and space flight, the estimation of

Table 4 Parameters values and discrepancies

Cell	Carrier flow rate (mg/s)	Carrier gas	Tracer	α_1	β_1	α_2	β_2	Injection-outlet surface correlation (%)	FTIR measured-Estimated surface correlation (%)
Class 3	50	N_2	CH_4	20	20.014	10	11.96	0.4	0.2
Class 3	100	N_2	CH_4	20	20.043	10	11.93	0.2	0.8
Class 40	50	N_2	CH_4	20	20.008	10	10.98	0.7	0.4
Class 40	100	N_2	CH_4	20	20.122	10	13.5	0.0	0.3
–	50	%	CH_4	20	19.995	10	11.3	0.3	1.4
–	50	$N_2 + CH_4$	N_2	20	19.979	10	12.6	0.4	−1.3
–	50	$N_2 + CH_4$	H_2	20	20.126	10	10.2	0.7	2.2

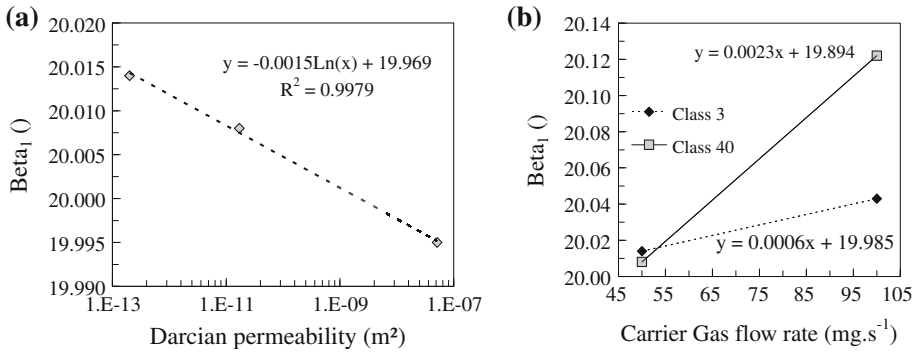

Fig. 14 Relationship of the parameter β_1 with the permeability (**a**) and carrier gas flow rate (**b**)

permeation properties of dedicated porous media such as some metallic or CMC materials is required. The community still faces a big lack in correct evaluation of permeability, particularly with interaction of heat and mass transfers. The experiments are generally conducted on-ground with dedicated test facility to acquire the mass flow rate through the porous media and the related pressure drop to determine the Darcian and Forchheimer terms. However, they use intermediate parameters such as dynamic viscosity and density which are not measured and which highly vary with pressure and temperature changes. This can introduce strong uncertainty and for this reason, a new methodology was proposed in this paper to avoid this problem. The permeability of porous materials changes due to the chemical phenomenon (coke formation) associated to multi-physics flow with pyrolysis. One of the advantages of the optical method presented in this study is to be able measuring the Darcian permeability during flight. The Infra Red signal of tracer injected through porous samples has been analyzed to link its characteristics to physical data before proposing the most relevant optical parameters and before linking them to Darcian permeability. The method is found to be applicable principally to low permeability material (with K_D lower than 10^{-13} m^2) except if large mass flow rates are provided for the test (in the order of 1 g s^{-1}). The peak width of the IR signal is the most relevant parameters and it has been linked to the Darcian term by linear equation. A further analytical work has been started to extend these first results. A difficulty to get a good agreement for both peak width and height is a strong limitation of the method. Nevertheless, the coefficient noted β_1 has been identified to be linked linearly to the Darcian term. The work will now be extended to a wider range of porous samples to validate and to improve the method. The data acquisition will be made with a single system to avoid the confusing problem of synchronization and the acquisition frequency will be strongly increased to get a better definition of the peak (at least 6 points per peak is preferable). A complementary analytical approach based on convolution products will be implemented to avoid arbitrary adjustment of some parameters.

Acknowledgments This work was supported by the ESA-ESTEC, Contract no.: 3-12861/09/NL/PA. The authors would like to sincerely thank J. Steelant from ESA, M. Bouchez and B. Le Naour from MBDA-and D. Blanc and D. Courilleau from the IUT Bourges.

References

1. M. Bouchez et al. Material-aero-thermal interaction computations in the ATLLAS European programme, AIAA-2008-4670 (2008)
2. M. Bouchez et al. Multi-level coupled simulations of cooled structures in the ATLLAS European programme, AIAA 2009-7355 (2009)
3. N. Gascoin et al. Permeation of inert and supercritical reactive fluids through metallic and composite media, AIAA-2010-6551 (2010)

4. T. Langener, J. von Wolfersdorf, T. Laux, J. Steelant, Experimental investigation of transpiration cooling with subsonic and supersonic flows at moderate temperature levels, AIAA 2008-5174 (2008)
5. J. Steelant, Achievements obtained on aero-thermal loaded materials for high-speed atmospheric vehicles within ATLLAS, AIAA-2009-7225 (2009)
6. G. Fau, N. Gascoin, P. Gillard, M. Bouchez, J. Steelant, Fuel pyrolysis through porous media: coke formation and coupled effect on permeability, 17th hypersonic. AIAA, San Francisco, 11–14th April (2011)
7. N. Gascoin, P. Gillard, M. Bouchez, Chemical composition and mass flow measurements in a supercritical reactive flow for hypersonic real-time application. Aerospace. Sci. Technol **14**, 266–275 (2010)
8. N. Gascoin, Pyrolysis of supercritical endothermic fuel: evaluation for active cooling instrumentation. IJCRE. 6 (2008)
9. N. Gascoin, P. Gillard, S. Bernard, M. Bouchez, Characterisation of coking activity during supercritical hydrocarbon pyrolysis. Fuel. Proc. Technol **89**, 12 (2008)
10. P. Habisreuther, N. Djordjevic, N. Zarzalis, Statistical distribution of residence time and tortuosity of flow through open-cell foams. Chem. Eng. Sci. 64 (2009)
11. J. Villermaux, Réacteurs Chimiques, Principe, Techniques de l'Ingénieur. J4010 (1994)
12. J.P. Moulin, D. Pareau, M. Rakib, M. Stambouli, Transfert de matière, Méthodologie, Techniques de l'Ingénieur. J1070 (2000)
13. J. Garcia-Serna et al. Modelling residence time distribution in chemical reactors: a novel generalised n-laminar model Application to supercritical CO2 and subcritical water tubular reactors, J. Supercrit. Fluids. 41 (2007)
14. A. Plugatyr, I. M. Svishchev, Residence time distribution measurements and flow modelling in a supercritical water oxidation reactor: Application of transfer function concept, J. Supercrit. Fluids. 44 (2008)
15. A. Buch, M. Rakib, M. Stambouli, Transfert de matière: Cinétique du transfert de matière entre deux phases, Techniques de l'Ingénieur, J1075 (2008)
16. E. Rodier, J.A. Dodds, D. Leclerc, G. Clément, Changes in fluid residence time distribution during deep-bed filtration, Chem. Eng. J. 68 (1997)
17. N. Gascoin, *Etude et mesure de paramètres pertinents dans un écoulement réactif application au refroidissement par endocarburant d'un super-statoréacteur*, First Edition, (Editions Universitaires Européennes, 2010), pp. 376
18. G. Abraham, Etude et développement d'une méthode d'analyse par spectroscopie infrarouge appliquée à la pyrolyse d'hydrocarbures en conditions supercritiques et transitoires, Ph.D. Thesis, University of Orléans, France (2009)